Lifetime measurements by the Doppler-shift attenuation method in the ^{115}Sn(α,$n\gamma$)^{118}Te reaction

C. Mihai,[1,2] A. A. Pasternak,[3] S. Pascu,[1] D. Filipescu,[1] M. Ivaşcu,[1] D. Bucurescu,[1] G. Căta-Danil,[1,4] I. Căta-Danil,[1] D. Deleanu,[1] D. G. Ghiţă,[1] T. Glodariu,[1] N. Mărginean,[1] R. Mărginean,[1] A. Negret,[1] T. Sava,[1] L. Stroe,[1] G. Suliman,[1] and N. V. Zamfir[1]

[1]*Horia Hulubei National Institute of Physics and Nuclear Engineering, RO-077125 Bucharest, Romania*

[2]*Faculty of Physics, University of Bucharest, Bucharest, Romania*

[3]*Cyclotron Laboratory, A.F. Ioffe Physical Technical Institute, 194021 St. Petersburg, Russia*

[4]*Physics Department, University "Politehnica" of Bucharest, Bucharest, Romania*

(Received 13 December 2010; revised manuscript received 19 April 2011; published 16 May 2011)

γ rays were measured at several angles in both singles and coincidence modes in the ^{115}Sn(α,$n\gamma$)^{118}Te reaction at 15 MeV on a thick target. Multipolarities and mixing ratios were determined from the γ-ray angular distribution analysis. Lifetimes of 11 low- and medium-spin excited states in ^{118}Te were determined from a Monte Carlo Doppler-shift attenuation method analysis of the Doppler broadened line shapes of γ rays deexciting the levels. The results are discussed in comparison with the predictions of the interacting boson model.

DOI: 10.1103/PhysRevC.83.054310 PACS number(s): 21.10.Tg, 23.20.Lv, 25.55.Hp, 27.60.+j

I. INTRODUCTION

At low spin, tellurium nuclei show a specific behavior of quadrupole vibrators, which is practically preserved along the whole isotopic chain. Besides this type of collective feature, intruder states are expected in such nuclei near (proton) shell gap. Such states arise from two-proton excitations from the $g_{9/2}$ shell across the $Z = 50$ closed shell, are more deformed than the "normal" low-lying, spherical states, and are lowest in energy in the middle of the shell (Refs. [1–3]). Such states were observed in Cd, Sn, Sb, and I isotopes (Refs. [1–4] and references therein) and are also expected to occur in Te isotopes. However, in Te isotopes, such deformed, rotational structures have been clearly observed only at higher spins where the bands are better defined [5,6], whereas at lower spins the observed structures are rather irregular and difficult to assign.

The nucleus ^{118}Te is in the middle of the neutron shell ($N = 66$), therefore one expects to have an intruder rotational band based on a low-lying 0^+ state. This idea appears to be supported by the fact that this isotope has the lowest-lying 0_2^+ state within the Te chain. On the other hand, on top of this state, one does not observe a regular band among the several known 2^+ and 4^+ excited states. At higher spins, there are regular bands which could be interpreted as being due to intruder states [6], but their continuation at lower spins is not obvious. One explanation could be that the intruder states are mixed with the normal ones, causing a distortion of both sequences. The systematics of the lower-spin states in the $^{116-124}$Te isotopes were reasonably well described in terms of mixed-configuration interacting boson model-2 (IBA-2) calculations, where two bosonic configurations differing by two in the total number of bosons are mixed [4].

To distinguish between states with strong intruder character and "normal" configuration states, and to understand their mixing, one needs comprehensive information on the electromagnetic transition probabilities between low-lying nonyrast states. These states are optimally populated through reactions using light projectiles (such as p, n, α) and their lifetimes can be measured using the Doppler-shift attenuation method (DSAM) (see Refs. [5,7–9]).

In the case of ^{118}Te, the lack of experimental information concerning the low-spin states prohibited such a detailed investigation. Previously, excited states in ^{118}Te [10] were populated and studied in the β^+ decay of ^{118}Sb [11,12], in (α,xn) reactions [1,13], and in heavy-ion induced reactions [6,14]. Information regarding lifetimes and electromagnetic transition probabilities in the ground-state band comes from a heavy-ion experiment [14]. No information on the lifetimes of low-lying nonyrast states exists. In the present work, excited states in ^{118}Te were populated through the ^{115}Sn(α,n)^{118}Te reaction at 15 MeV bombarding energy. Level lifetimes were extracted by the DSAM, from the analysis of the experimental γ-ray line shapes.

The small recoil velocities (typically $v/c \sim 0.3\%$, corresponding to recoil energies of ~500 keV) and the side-feeding pattern of the (α,n) reaction make the application of the DSAM in this case difficult. However, as shown in a previous publication [9], a correct treatment of the level side feedings enables a reliable extraction of the lifetimes. In Sec. II some details of the method are discussed. Section III presents the results of the measurements. In the last section, a discussion of the electromagnetic transition probabilities is made in comparison with predictions of the interacting boson approximation (IBA).

II. EXPERIMENTAL ARRANGEMENT

Excited states of ^{118}Te were populated in the ^{115}Sn(α,n)^{118}Te reaction, induced by a 15 MeV, 2 pnA ^{4}He^{+2} beam delivered by the Bucharest FN tandem accelerator on a 3.7 mg/cm^2 tin foil, and studied by γ-ray spectroscopy. The target had a 51.2% enrichment in ^{115}Sn and contained other tin isotopes as well: 24.4% ^{116}Sn, 5.4% ^{117}Sn, 7.4%

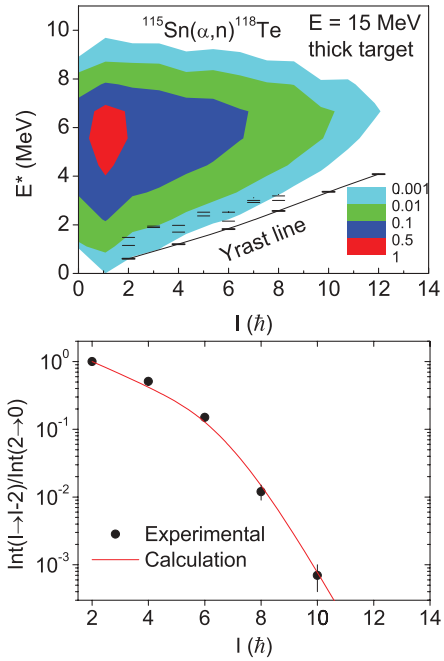

FIG. 1. (Color online) Top: Entry state population of ^{118}Te, populated in the ^{115}Sn(α,n) reaction at 15 MeV, calculated with the COMPA code. The slowing down of the α-particle beam in the thick target is taken into account. Some 10^6 Monte Carlo events were simulated. Both yrast levels and known levels above the yrast line are shown. Yrast line approximation is $E^*_{yr} = 0.02725 + 0.25787I + 0.00759I^2$. Bottom: Experimental (circles) and calculated (solid line) distribution of normalized intensities along the yrast line of ^{118}Te, populated in the reaction ^{115}Sn(α,n) at 15 MeV.

^{118}Sn, 1.9% ^{119}Sn, and 6.7% ^{120}Sn. The γ rays were detected using an array of seven 55% efficiency high-purity germanium (HPGe) detectors, five placed in a ring at 37° with respect to the beam axis in the backward direction, one at 90°, and one movable in the forward direction. The γ-ray spectra were calibrated using standard ^{152}Eu and ^{60}Co sources, and the gain stability during the experiment was monitored using a weak ^{60}Co source conveniently placed near the reaction chamber. The data were recorded in both singles and coincidence list modes. In the latter case, the trigger condition was that two γ rays were detected in coincidence. The singles spectra were used for line-shape and angular distribution analysis, while the lower statistics coincidence data were used to check feeding relationships and also for line-shape analysis of γ-ray transitions affected by the presence of strong contaminant peaks. The angular distribution of γ-ray intensities in the singles spectra, measured at six angles between 10° and 90° were used to extract the intensity of the transitions and the $E2/M1$ mixing ratios δ when the measured points had a small uncertainty.

TABLE I. Level lifetimes in ^{118}Te as measured in the present work. For each level, the γ-ray transition used for the DSAM analysis is mentioned.

E_{level} (keV)	J^π	E_γ (keV)	τ (ps)
1150.8	2^+_2	1150.8[a]	$1.2^{+0.4}_{-0.2}$
1482.1	2^+_3	1482.1[a]	$0.9^{+0.4}_{-0.2}$
1702.7	4^+_2	551.8[a]	>1
1891.9	3^+_1	1286.3[a]	>2.5
1944.5	3^-_1	1338.8[b]	0.95 ± 0.20
1976.1	4^+_3	770.0, 1370.4[b]	$1.0^{+0.3}_{-0.2}$
2020.6	$(2^+,3^+)$	869.4, 1414.9[a]	$0.35^{+0.30}_{-0.15}$
2150.2	6^+_2	943.7[a]	$1.0^{+0.4}_{-0.3}$
2367.8	5^+_1	1161.2[a]	$1.3^{+0.6}_{-0.3}$
2571.2	(5^-_1)	1364.7[b]	$0.45^{+0.16}_{-0.12}$
2573.9	8^+_1	753.0[b]	$0.95^{+0.35}_{-0.20}$
2999.7	7^-_1	1179.0[b]	$0.70^{+0.20}_{-0.15}$

[a]Evaluated from the spectra at 10°, 37°, and 53°.
[b]Evaluated from the spectra at 10°, 37°, 53°, and 90°.

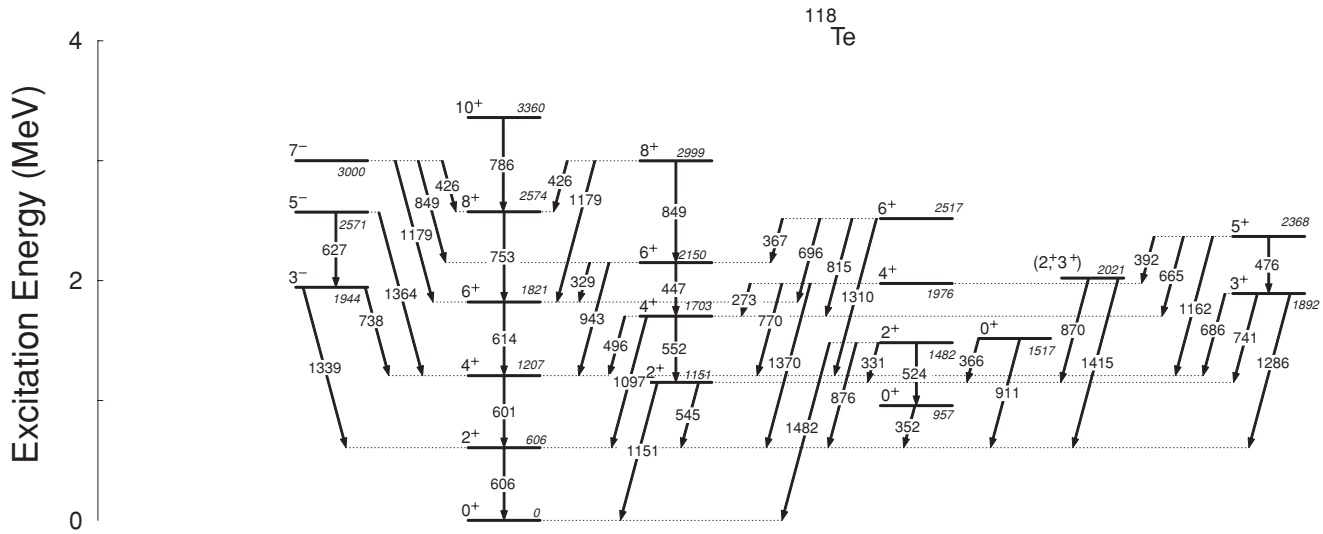

FIG. 2. Level and γ-ray decay scheme of ^{118}Te. This is only a qualitative drawing showing levels for which new information was obtained in the present work and levels that are discussed in Sec. IV.

TABLE II. Experimental characteristics of γ-ray transitions in ^{118}Te as determined in the present work. The transition probability $B(\sigma\lambda)$ values contain also a 15% uncertainty due to the uncertainty in the stopping power. For the procedure of calculating the errors of the $B(\sigma\lambda)$ values, see Ref. [9]. The subscript of the spin value is the experimental level order number.

E_{level} (keV)	τ (ps)	E_γ (keV)	$J_i^\pi \rightarrow J_j^\pi$	I_γ	a_2	a_4	δ	$\sigma\lambda$	$B(\sigma\lambda)$ (W.u.)
605.7	8.8 ± 1.4[a]	605.7	$2_1^+ \rightarrow 0_1^+$	100 ± 5	0.16(1)	−0.07(1)		$E2$	33^{+6}_{-5}
1150.8	$1.2^{+0.4}_{-0.2}$	545.1	$2_2^+ \rightarrow 2_1^+$	18 ± 2	−0.01(1)	−0.04(1)	-0.35 ± 0.02	$M1$	$9.5^{+3.5}_{-2.1} \times 10^{-2}$
								$E2$	28^{+13}_{-7}
							$11.0^{+0.7}_{-0.5}$	$M1$	$8.5^{+3.5}_{-2.8} \times 10^{-4}$
								$E2$	264^{+100}_{-57}
		1150.8	$2_2^+ \rightarrow 0_1^+$	5.1 ± 0.6	0.18(2)	−0.07(2)		$E2$	$1.8^{+0.7}_{-0.4}$
1206.4	4.4 ± 0.8[a]	600.7	$4_1^+ \rightarrow 2_1^+$	52 ± 2	0.26(1)	−0.09(1)		$E2$	69^{+19}_{-11}
1482.1	$0.9^{+0.4}_{-0.2}$	331.0	$2_3^+ \rightarrow 2_2^+$	0.3 ± 0.1[a]	0.11(5)	−0.06(6)	-0.25 ± 0.05	$M1$	$2.4^{+1.8}_{-0.9} \times 10^{-2}$
								$E2$	$9.5^{+8.5}_{-3.5}$
							4.4 ± 0.3	$M1$	$1.2^{+0.9}_{-0.5} \times 10^{-3}$
								$E2$	166^{+119}_{-61}
		524.4	$2_3^+ \rightarrow 0_2^+$	1.0 ± 0.2[a]	0.17(7)	−0.07(5)		$E2$	60^{+35}_{-17}
		876.4	$2_3^+ \rightarrow 2_1^+$	6.5 ± 0.5	−0.03(1)	−0.04(2)	-0.36 ± 0.02	$M1$	$2.8^{+1.4}_{-0.6} \times 10^{-2}$
								$E2$	$3.4^{+1.9}_{-0.9}$
							16.0 ± 2	$M1$	$1.3^{+0.6}_{-0.5} \times 10^{-4}$
								$E2$	30^{+16}_{-7}
		1482.0	$2_3^+ \rightarrow 0_1^+$	0.6 ± 0.1				$E2$	$0.20^{+0.11}_{-0.05}$
1702.7	>1	496.8	$4_2^+ \rightarrow 4_1^+$	3 ± 1[c]	0.12(5)	−0.06(2)	1.72 ± 0.08	$M1$	<0.018
								$E2$	<160
		551.8	$4_2^+ \rightarrow 2_2^+$	5.4 ± 0.4	0.27(2)	−0.12(2)		$E2$	<210
		1097.5	$4_2^+ \rightarrow 2_1^+$	0.8 ± 0.2[d]				$E2$	<1.1
1820.8	3.4 ± 0.5[a]	614.4	$6_1^+ \rightarrow 4_1^+$	15 ± 1	0.31(1)	−0.11(1)		$E2$	80^{+14}_{-10}
1891.9	>2.5	685.2	$3_1^+ \rightarrow 4_1^+$	1.0 ± 0.1	0.10(9)	−0.05(11)	0.45 ± 0.29	$M1$	$<1 \times 10^{-2}$
								$E2$	<4.5
		741.2	$3_1^+ \rightarrow 2_2^+$	2.4 ± 0.1	−0.04(3)	0.01(3)	0.16 ± 0.02	$M1$	$<1.8 \times 10^{-2}$
								$E2$	<0.7
		1286.3	$3_1^+ \rightarrow 2_1^+$	1.2 ± 0.1	0.04(6)	0.01(8)	0.20 ± 0.04	$M1$	$<1.6 \times 10^{-3}$
								$E2$	<0.036
1944.5	0.95 ± 0.20	738.1	$3^- \rightarrow 4_1^+$	0.15 ± 0.03[b]				(E1)	$3.5^{+1.7}_{-0.9} \times 10^{-5}$
		793.7	$3^- \rightarrow 2_2^+$	0.05 ± 0.01[b]				(E1)	$9.4^{+4.5}_{-2.3} \times 10^{-6}$
		1338.8	$3^- \rightarrow 2_1^+$	3.9 ± 0.2	−0.21(2)	0.04(3)		$E1$	$1.6^{+0.6}_{-0.3} \times 10^{-4}$
1976.1	$1.0^{+0.3}_{-0.2}$	273.1[h]	$4_3^+ \rightarrow 4_2^+$	0.23 ± 0.05				$M1$	$5.3^{+2.7}_{-1.5} \times 10^{-2}$
								$E2$	529^{+281}_{-145}
		770.0	$4_3^+ \rightarrow 4_1^+$	2.2 ± 0.2	−0.02(5)	−0.11(6)	$+3.4^{+0.3}_{-0.2}$	$M1$	$1.7^{+0.9}_{-0.4} \times 10^{-3}$
								$E2$	27^{+11}_{-6}
		1370.4	$4_3^+ \rightarrow 2_1^+$	3.2 ± 0.3	0.25(6)	−0.09(7)		$E2$	$2.4^{+1.0}_{-0.6}$
2020.6	$0.35^{+0.30}_{-0.15}$	869.7	$(2^+,3^+) \rightarrow 2_2^+$	0.5 ± 0.1	0.25(26)	0.12(32)	$+6.0 \pm 0.3$[i]	$M1$	$4.3^{+4.8}_{-1.7} \times 10^{-4}$
								$E2$	13^{+17}_{-4}
		1414.9	$(2^+,3^+) \rightarrow 2_1^+$	2.2 ± 0.2	0.04(20)	0.02(23)		$M1$	$1.5^{+1.6}_{-0.4} \times 10^{-2}$
2150.2	$1.0^{+0.4}_{-0.3}$	329.3	$6_2^+ \rightarrow 6_1^+$	2.2 ± 0.2	0.22(3)	−0.05(4)	-0.3 ± 0.2	$M1$	$0.27^{+0.17}_{-0.06}$
								$E2$	<80
		447.4	$6_2^+ \rightarrow 4_2^+$	0.4 ± 0.1[e]				$E2$	82^{+58}_{-26}

TABLE II. (*Continued*)

E_{level} (keV)	τ (ps)	E_γ (keV)	$J_i^\pi \rightarrow J_j^\pi$	I_γ	a_2	a_4	δ	$\sigma\lambda$	$B(\sigma\lambda)$ (W.u.)
		943.7	$6_2^+ \rightarrow 4_1^+$	2.6 ± 0.3	0.34(8)	−0.09(0)		$E2$	13^{+8}_{-3}
2367.8	$1.3^{+0.6}_{-0.3}$	391.8	$5_1^+ \rightarrow 4_3^+$	0.10 ± 0.02[d]				$M1$	$1.2^{+0.8}_{-0.4} \times 10^{-2}$
		475.8	$5_1^+ \rightarrow 3_1^+$	0.6 ± 0.1[f]	0.22(6)	−0.07(7)		$E2$	134^{+77}_{-35}
		665.1	$5_1^+ \rightarrow 4_2^+$	0.4 ± 0.1[g]			$+0.9^{+1.3}_{-0.4}$[b]	$M1$	$1.6^{+4.4}_{-0.7} \times 10^{-3}$
								$E2$	10^{+8}_{-5}
		1161.2	$5_1^+ \rightarrow 4_1^+$	1.4 ± 0.1	0.19(8)	−0.12(10)	$+7.0^{+0.9}_{-0.3}$	$M1$	$1.2^{+0.7}_{-0.3} \times 10^{-4}$
								$E2$	$3.6^{+1.9}_{-0.9}$
2571.2	$0.60^{+0.20}_{-0.15}$	626.7	$(5_1^-) \rightarrow 3_1^-$	0.5 ± 0.1[d]	0.24(4)	−0.11(5)		$E2$	104^{+64}_{-28}
		1364.7	$(5_1^-) \rightarrow 4_1^+$	1.6 ± 0.2				$(E1)$	$2.2^{+1.2}_{-0.5} \times 10^{-4}$
2573.9	$1.10^{+0.35}_{-0.25}$[g]	753.0	$8_1^+ \rightarrow 6_1^+$	1.1 ± 0.1	0.25(7)	−0.14(8)		$E2$	76^{+33}_{-17}
2999.7	$0.70^{+0.20}_{-0.15}$	426.1	$7_1^- \rightarrow 8_1^+$	0.02 ± 0.01[d]				$E1$	$2.1^{+1.0}_{-0.5} \times 10^{-4}$
		850.1	$7_1^- \rightarrow 6_2^+$	0.11 ± 0.03[d]				$E1$	$1.2^{+0.5}_{-0.3} \times 10^{-4}$
		1179.3	$7_1^- \rightarrow 6_1^+$	0.6 ± 0.03	−0.37(14)	0.17(17)		$E1$	$2.5^{+1.1}_{-0.5} \times 10^{-4}$

[a]Lifetimes from Ref. [14].
[b]From Ref. [10].
[c]Branching ratio adopted from Refs. [6,10] and this work.
[d]Branching ratio from Ref. [6].
[e]Branching ratio from Ref. [6] and this work.
[f]Branching ratio from Refs. [6,10].
[g]Lifetime adopted from Refs. [6,10] and this work.
[h]Previously unknown transition.
[i]Evaluated assuming $J^\pi = 3^+$.

III. EXPERIMENTAL RESULTS

A. DSAM analysis

The application of the DSAM for the (α,n) reaction on relatively heavy target nuclei ($A \geqslant 100$) has some specific advantages compared to the heavy-ion (HI) induced reactions: (i) low and intermediate spin states above the yrast line are more strongly populated, (ii) the influence of cascade feeding from discrete levels above is much smaller, (iii) side feeding is realized mainly by fast statistical $E1$ transitions from the entry state continuum, and (iv) due to the small amount of open reaction channels at low beam energies, high-statistic single γ-ray spectra are clean and suitable for the line-shape analysis. In our case, however, the strong contamination of the target with other isotopes limited the analysis to intense transitions that did not overlap with transitions from other reaction channels.

The main disadvantages of using the DSAM in the (α,n) reaction are as follows: (i) relatively small recoil velocities (typically $v/c \sim 0.3\%$) resulting in a small Doppler effect, which is smaller than the resolution of HPGe detectors even for $E_\gamma \geqslant 1$ MeV; therefore, the method sensitivity relies on good energy resolution of the HPGe detectors ($\leqslant$2 keV at 1.332 MeV) and well-defined instrumental line shapes; (ii) the role of cascade feeding is rather small so that well-known special gating techniques (flight gate transition above and narrow gate transition below) cannot be applied; and (iii) at these recoil energies, the nuclear component of the recoil stopping power is dominant, which results in the fast slowing down of the recoils in the target (stopping time t_{st} is typically less than 0.5 ps), thus making measurements of lifetimes with $\tau \geqslant 1$ ps very difficult; and (iv) even relatively short effective side feeding times ($\approx$0.1–0.2 ps), being comparable with t_{st}, can drastically disturb the results of lifetime determinations, therefore the side feeding pattern should be carefully taken into account.

The present analysis of the experimental DSAM line shapes is similar to that described in detail in Ref. [9]. It was carried out using updated versions of the Monte Carlo codes COMPA, GAMMA, and SHAPE, which are described in some detail in Refs. [15–17] and were widely used before for α-particle and HI induced reactions (latest publications are Refs. [9,18–22]). This software includes the Monte Carlo simulation of the production and slowing down of recoils as well as that of the γ-ray emission and detection. The COMPA program simulates the reaction kinematics, the slowing down of the projectiles in the target, the formation of the compound nuclei, the particle emission, and the entry state population distributions. In the GAMMA program, the slowing-down process and multiple scattering of the recoils in the target, the emission of γ-ray cascades from the entry states to the level of interest, and the detection of the γ quanta in the detector system are simulated. In the calculation of Doppler broadened line shapes, not only the cascade feeding through all known levels is taken into account but also the side feeding cascades from each entry state. In the SHAPE code, the Doppler affected

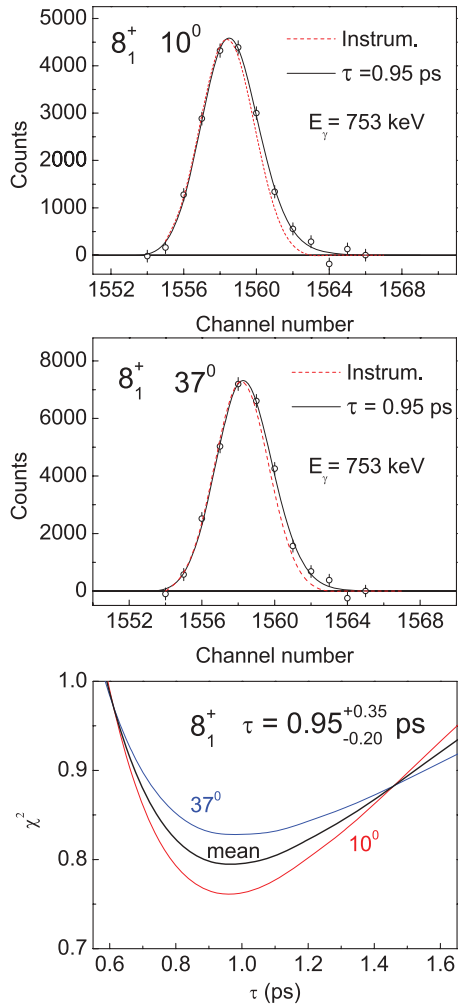

FIG. 3. (Color online) DSAM line-shape analysis of the 753 keV, $8_1^+ \rightarrow 6_1^+$ transition. The dotted lines in the upper panels correspond to the instrumental line shape, the solid lines are calculated for $\tau = 0.95$ ps. The χ^2 analysis is presented in the bottom panel and reflects only the statistical error.

line shapes resulting from the experiment are fitted with calculated ones, taking into account the instrumental line shapes of the detectors. Up to seven overlapping peaks can be simultaneously fitted, which may have Doppler affected or instrumental line shapes, using lifetimes, positions, and relative areas as parameters.

The distribution of ^{118}Te entry states (i.e., states populated after neutron emission, before γ cascades) for the ^{115}Sn(α,n) reaction at 15 MeV incident energy, calculated with the COMPA code, is presented in the top of Fig. 1. The slowing down of the α-particle beam in the thick target was taken into account. Along with the yrast line, the known levels above yrast are shown. As can be seen from this figure, the population probability has a maximum at spins $I = 1$–$2\,\hbar$ and sharply decreases with increasing spin. This distribution is drastically different from the corresponding one calculated for the ^{109}Ag(^{13}C, $p3n$)^{118}Te reaction at $E = 54$ MeV [14], where the maximum was located near $I = 10\,\hbar$.

The entry states are the starting points of side feeding γ-ray cascades, which are simulated by the GAMMA code. The competition between statistical $E1$, $M1$, and $E2$, as well as stretched $E2$ and $M1$ transitions defines the distribution of side feeding times t_{sf}, that is, the times which are needed for the cascade to reach the destination level from the entry state. Simultaneously with t_{sf}, other features of the cascades such as multiplicity distribution and the distribution of intensities along the yrast band are calculated. The side feeding model is briefly described in Ref. [17]. In that paper, dedicated to the investigation of the ^{122}Sn(^{14}N,5n)^{131}La reaction at $E = 70$ MeV, the comparison of experimental and calculated populations of the yrast band levels was used for the determination of the side feeding model parameters, later used to take into account the side feeding delay times in DSAM lifetime measurements. A similar method was also used for the investigation of chiral bands in ^{128}Cs, populated in the ^{122}Sn(^{10}B, 4n) reaction [23]. As it turned out, in these reactions both the intensity and time distributions are mainly defined by features of stretched $E2$ and $M1$ transitions and depend only slightly on statistical transitions.

Experimental and calculated (by the GAMMA program) intensities of $I \rightarrow I - 2$ transitions along the yrast line of ^{118}Te, normalized to the $2_1^+ \rightarrow 0_1^+$ transition, are presented in the bottom panel of Fig. 1. A good agreement between experiment and the model prediction was observed practically independently of the side feeding model parameters. This fact can be explained by the dominant role of the statistical (mainly $E1$) transitions in the side feeding pattern, which practically does not change spin values of the entry state after the γ cascade. Therefore, the calculated distribution mainly reflects the entry state distribution, and Fig. 1 shows that the compound nucleus formation as well as the neutron evaporation pattern, calculated by COMPA, are confirmed by experiment.

In this situation, only those experimental data that are connected with the time evolution of side feeding cascades are useful for the evaluation of the statistical cascade parameters. Useful information could be a comparison of absolute level lifetimes, measured in conditions where the side feeding is absent [such as Coulomb excitation or the (n,n') reaction], with lifetimes measured by DSAM in the (α,n) reaction. This was done in the case of ^{122}Te [9], but it is impossible to do so in the present case of the unstable ^{118}Te. So, only some indirect data can be extracted. Since, in the first place, the $E1$ statistical transitions strength f_{E1} is important, the corresponding parameter of the $E1$ giant resonance σ_0 can be used for the comparison with experiment. In the programs COMPA and GAMMA the following approximation for near-spherical nuclei with $A > 50$ is used [24,25]:

$$f_{E1} = (8.7 \times 10^{-8})\sigma_0 E_\gamma^2 \Gamma_0^2 / \left[\left(E_\gamma^2 - E_0^2\right)^2 + E_\gamma^2 \Gamma_0^2\right], \qquad (1)$$

where $E_0 = 50/A^{0.24}$, $\Gamma_0 = 0.3E_0$, and $\sigma_0 = 10.6A/\Gamma_0 = 0.707A^{1.24}$. For ^{118}Te, $E_0 = 15.9$ and $\Gamma_0 = 4.8$, and thus the "standard" value of σ_0 is 262. For the neighboring nuclei ^{119}I and ^{120}Xe, populated in the reactions ^{109}Ag(^{13}C, 3n) and ^{111}Cd(^{12}C, 3n), respectively, effective side feeding times $\tau_{\text{eff}} = \langle t_{sf} \rangle$ have been measured by DSAM [26,27]. Since these data were obtained for high spin state regions $I = 39/2\hbar$ and

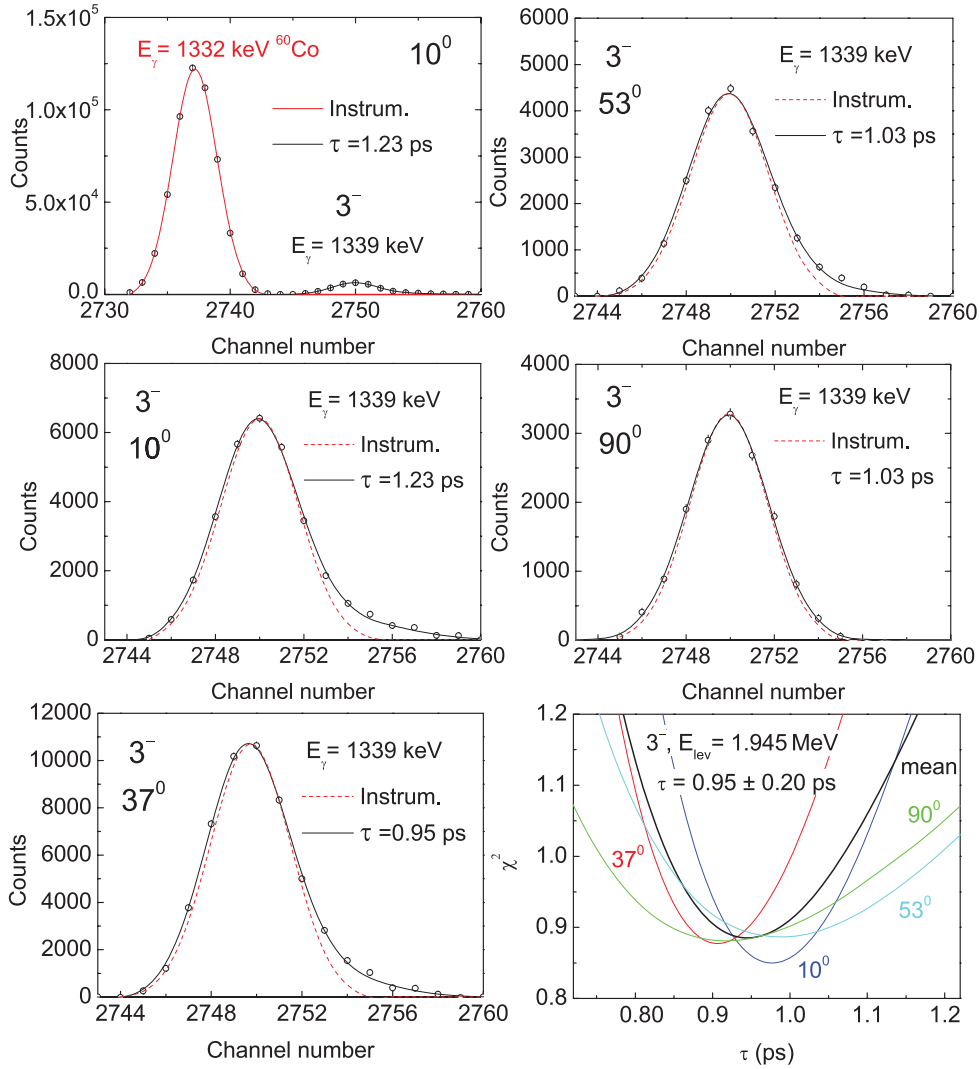

FIG. 4. (Color online) Line-shape analysis of the 1339 keV transition from the 3_1^-, 1945 keV state. This line is situated near the 1332 keV line of the ^{60}Co calibration source. Left top panel shows the two peaks and the solid line is calculated for $\tau = 1.23$ ps and includes the instrumental line shape. Solid lines in the other panels with the 1339 keV line-shape analysis are calculated for the indicated τ values, and the instrumental line shape is shown by the dotted line. The right bottom panel shows χ^2 plots and the evaluation of the adopted lifetime value.

$I = 18\hbar$, respectively, where side feeding is mainly realized by statistical cascades, τ_{sf} can be regarded as suitable for the σ_0 evaluation. To evaluate σ_0, calculated $\tau_{eff}(\sigma_0)$ dependencies were compared with the experimental values of τ_{sf}. As already mentioned, more direct data were obtained for ^{122}Te [9] by comparing lifetimes measured in the (α,n) reaction with DSAM lifetimes measured in the $(n,n'\gamma)$ reaction [8]. In this case, the adopted value of $\sigma_0 = 273 \pm 50$ MeV^{-1} was the same as the "standard" model prediction. Therefore, for ^{118}Te we have also adopted the "standard" value of $\sigma_0 = 262$. This choice agrees with the values obtained for neighboring nuclei with heavy-ion reactions (which have, nevertheless, large errors). A 15% uncertainty arising from σ_0 evaluation was taken into account in the final error of the deduced lifetimes. This uncertainty reflects possible fluctuations in the dependence of f_{E1} on the mass number, which may be quite significant, as known from previous studies [24,28].

To evaluate the stopping power of the recoils, the Lindhard correction factors for the electronic (f_e) and nuclear (f_n) components were measured by line-shape analysis for the ^{119}I recoils traveling into a ^{109}Ag target [15]. Values of $f_e = 1.27 \pm 0.07$ and $f_n = 0.77 \pm 0.07$ were adopted for the ^{118}Te recoils [14] and were also used in this work.

B. Lifetime results

For an easy presentation of the measurements and their results, Fig. 2 shows the known levels of ^{118}Te [10] for which information on the lifetimes could be obtained in the present work. The lifetimes determined from the DSAM line-shape analysis are presented in Table I. Altogether, lifetime values or their lower limits could be determined for 12 excited states. The highest energy γ-ray branches of these levels were generally used for the DSAM analysis.

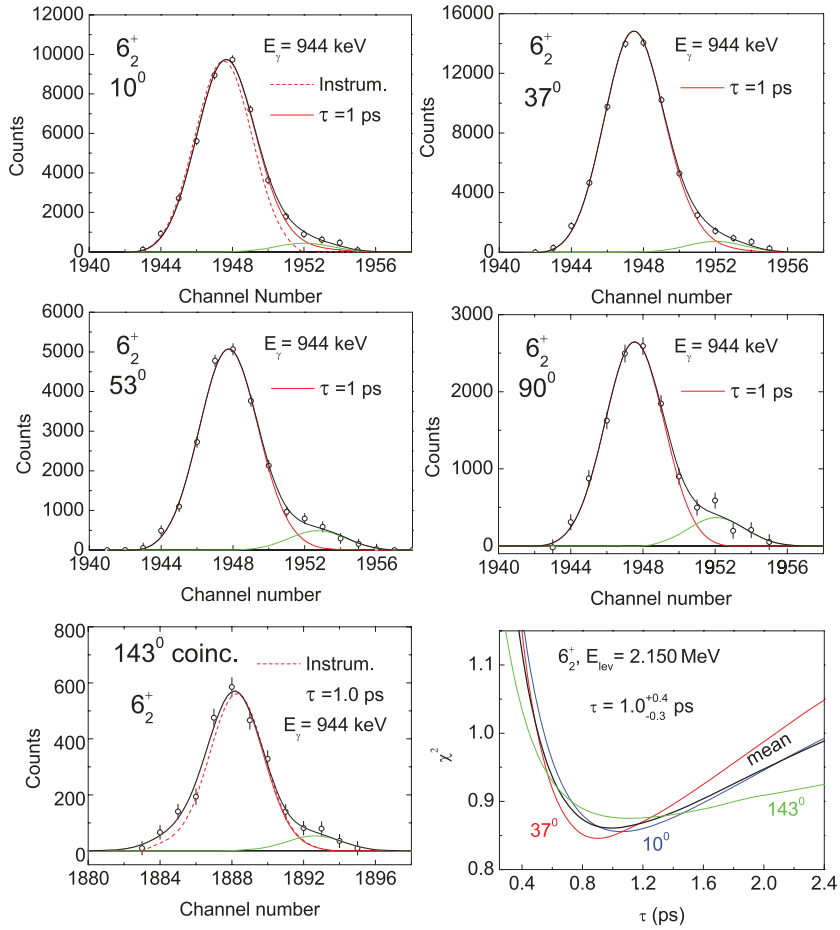

FIG. 5. (Color online) Line-shape analysis of the 944 keV transition from the 6_2^+, 2150 keV state. The dotted line in the left top panel corresponds to the instrumental line shape, while solid lines are calculated for $\tau = 1.0$ ps. A weak contamination peak is shown also as a solid line. The χ^2 analysis was performed for the 10°, 37°, and 143° spectra, the latter being obtained in coincidence (see text).

The transitions from the 2999.4 keV, 8_2^+ and 2999.7 keV, 7_1^- levels to the 6_1^+ state form an unresolved doublet at 1179 keV; however, the strong dipolar character of the angular distribution of this γ ray (see Table II) favors the assignment of the lifetime to the 7_1^- state at 2999.7 keV. Uncertainties of the lifetime values from Table I include statistical and side feeding contributions.

Examples of line-shape analysis for a few important cases, which illustrate special features of the DSAM application for $(\alpha,n\gamma)$ reactions, are presented below. Many more different examples, including levels with large cascade feedings and analysis of regions with many overlapping peaks, are given in our previous work [9].

The line-shape analysis of the 753 keV transition from the 8_1^+, 2574 keV state is shown in Fig. 3. The Doppler broadening of this line is smaller than that for the ^{109}Ag(^{13}C, $p3n$) reaction [14], but at the forward angles of 10° and 37° it is remarkable enough for a reliable lifetime measurement. The determined lifetime value, $\tau = 0.95^{+0.35}_{-0.20}$ ps, is in reasonable agreement with the values obtained by the DSAM and the plunger method in Ref. [14] ($\tau = 1.2^{+0.4}_{-0.3}$ ps) and by the DSAM in Ref. [29] ($\tau = 1.3^{+0.5}_{-0.4}$ ps).

The 1339 keV γ ray, corresponding to a transition from the 3_1^- level at 1945 keV excitation, is located near the 1332 keV line of the ^{60}Co source used for calibration. The left top panel of Fig. 4 shows these lines and illustrates the high quality of the instrumental line-shape calibration, which is very important for the line-shape analysis at small Doppler effect. The rest of the panels with the 1339 keV line shapes illustrate the comparison of calculated and instrumental line shapes at different angles. In this case, all spectra are suitable for χ^2 analysis, and the χ^2 plots give a reliable adopted result.

Figure 5 illustrates the case of the 944 keV transition from the 6_2^+ level at 2150 keV. This transition is not fully resolved from a weak neighboring line. In this case, the line shape shown at 143° was obtained in coincidence with the 849 keV transition (Fig. 2).

The 1364 keV γ ray corresponding to the transition $5^- \rightarrow 4_1^+$ from the 2571 keV level was found to contain 30% of the transition $4_3^+ \rightarrow 2_1^+$ in ^{120}Te, and the DSAM analysis took into account the contribution of that state, whose lifetime was determined in a separate experiment [30].

Besides the lifetimes given in Table I, and those of the yrast states (g.s.b.) both below and above the 8_1^+ state [14], only the lifetime of the 0_2^+ state at 957.5 keV was reported before, as $\tau = 79 \pm 65$ ps [10].

C. Angular distribution results

For the angular distribution measurements, the HPGe detector kept fixed at 90° with respect to the beam axis was used for normalization, while the mobile detector in

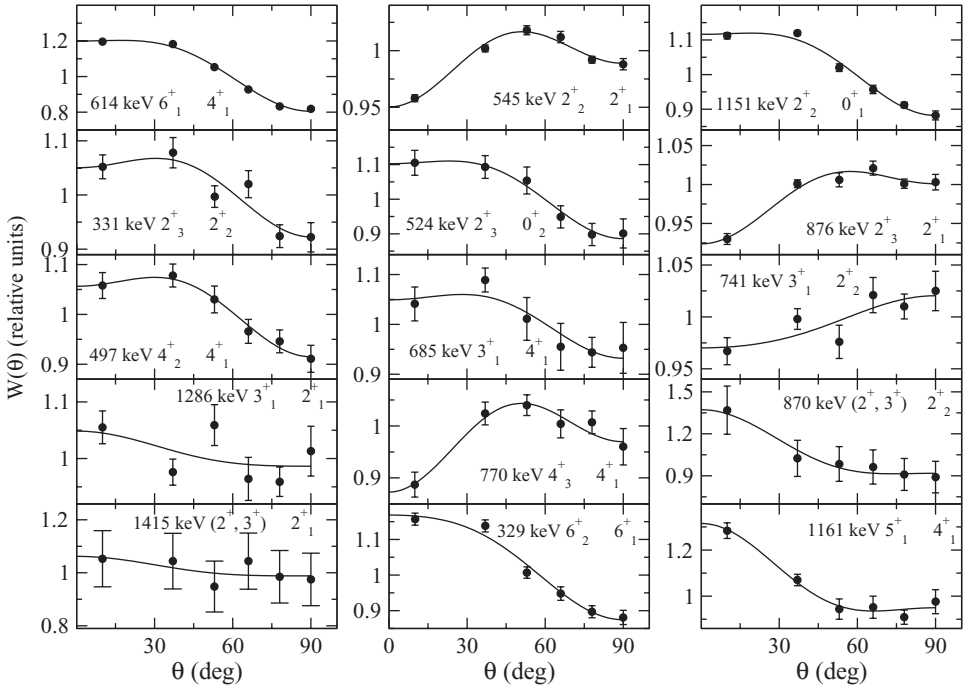

FIG. 6. Examples of angular distribution data for several γ-ray transitions. The experimental points are fitted with $W(\theta) = A_0[1 + a_2P_2(\cos\theta) + a_4P_4(\cos\theta)]$ (continuous curves) and the coefficients a_2 and a_4 are given in Table II.

the forward direction was positioned at six angles (10°, 37°, 53°, 66°, 78°, 90°), the γ-ray spectra being recorded in both singles and coincidence modes. The experimental angular distributions were fitted with the standard function $W(\theta) = A_0[1 + a_2P_2(\cos\theta) + a_4P_4(\cos\theta)]$. The angular distributions were also analyzed considering as fit parameters the mixing ratio $\delta(E2/M1)$ and the degree of state alignment σ which is the width of a Gaussian function describing the distribution of the magnetic substate population [31]. In Fig. 6, some of the fits to the measured γ-ray angular distributions are presented. The degree of alignment was estimated on a level-by-level basis, by analyzing the pure transitions deexciting the level of interest. The results of this analysis are included in Table II. The branching ratios determined on the basis of our γ-ray intensities agree reasonably well with those given in Ref. [6]. A previously unknown branch, of 273.1 keV, was observed for the decay of the 1976.1 keV, 4_3^+ state, toward the 4_2^+ state at 1702.7 keV.

D. Experimental transition probabilities

The reduced electromagnetic transition probabilities extracted from our data are also presented in Table II, including some results from Ref. [14] that are important for the discussion in the next section. A 15% error arising from recoil stopping power uncertainty is also taken into account in the Monte Carlo calculation of errors in $B(\sigma, \lambda)$ (similar to Ref. [9]). The procedure of deducing the substate alignment and mixing ratio was inconclusive for some transitions from the 2_2^+ state at 1151 keV and the 2_3^+ state at 1482 keV. As a result of this, in Table II, there are two possible values for the mixing ratio of three mixed transitions deexciting these levels. For the 876 keV $2_3^+ \rightarrow 2_1^+$ transition, the value $\delta = -0.36 \pm 0.02$ is close to the one given in the Evaluated Nuclear Structure Data File (ENSDF) [10] of $-0.58^{+0.05}_{-0.08}$. For the other two transitions, there is some preference for the lower δ values (see the discussion in Sec. IV). The transition probabilities of the positive-parity states will be discussed in detail later. For the negative-parity states 3^-, 1944.5 keV and 5^-, 2571.2 keV, the $B(E1)$ values deduced from the measured lifetimes (Table II) are very similar to those known for the corresponding states in ^{122}Te [32].

IV. DISCUSSION

The occurrence of intruder states in the Cd and Sn isotopes suggests that, by analogy, such states should appear also in the Te isotopic chain. Although the energy level systematics in Te isotopes have a different pattern if compared with Cd and Sn isotopes, the strong dependence of the energy of the first excited 0^+ state on the neutron number (with a pronounced minimum at $N = 66$) was taken as a hint that this state has an "intruder" character and should be the head of a deformed rotational band [4]. However, such a rotational band was not put into evidence in any of the tellurium isotopes. It is argued in Ref. [4] that the mixing between the normal and intruder configurations would strongly affect the members of both configurations, obscuring the appearance of a rotational band having as bandhead the first excited 0^+ state. This mixing is predicted to affect also the $B(E2)$ transition strengths for nonyrast levels, leading to values well outside the vibrational limit.

The mixed-configuration IBA-2 approach was applied to the $^{112-128}$Te isotope chain in Ref. [4] in order to take into account the predicted mixing between normal and intruder configurations. In this approach, the normal configuration states (with $N = N_\nu + 1$ bosons, where N_ν is the number of neutron bosons in Te) are mixed with an intruder

configuration, having $N_\nu + 3$ bosons. This approach provided a good description of the levels known at the time, among which were the 0^+ and 2^+ states, and claimed the largest percentage of intruder configuration in the 0_2^+ and 2_2^+ states of ^{116}Te and ^{118}Te [4].

Important information on the nature of the 0^+ states are their $E0$ strengths. Relative $E0$ strengths for the $^{118-122}$Te isotopes were measured in the β^+ decay of $^{118-122}$I in Ref. [11]. The relative $E0$ strengths for the 0_2^+ state in the above-mentioned isotopes have values close to the vibrational limit, while the values for the 0_3^+ are larger. This behavior was attributed to the mixing between the 0_2^+ and 0_3^+ states, a strong argument for this interpretation being the relatively intense $E0$ transition between them.

In the following, the absolute electromagnetic transition rates experimentally determined in the present work will be compared with predictions of theoretical model calculations.

We performed calculations with the interacting boson model-1 (IBA-1) [33]. By comparing with IBA-1 predictions,

TABLE III. Comparison between the experimental and calculated (IBA-1 model) level γ-ray transition probabilities. For the transitions $2_2^+ \to 2_1^+$, $2_3^+ \to 2_1^+$, and $2_3^+ \to 2_2^+$, the experimental $B(\sigma\lambda)$ values corresponding to the two possible mixing ratios of Table II are given.

Exp.					IBA-1		
E_{level} (keV)	Transition (keV)	$J_i^\pi \to J_f^\pi$	$B(M1)$ (W.u.)	$B(E2)$ (W.u.)	E_{level} (keV)	$B(M1)$ (W.u.)	$B(E2)$ (W.u.)
605.7	605.7[a]	$2_1^+ \to 0_1^+$		33^{+6}_{-5}	609.7		33
957.5[b]	351.7	$0_2^+ \to 2_1^+$		54 ± 45	1022.5		71
1150.8	545.1	$2_2^+ \to 2_1^+$	$9.5^{+3.5}_{-2.1} \times 10^{-2}$	28^{+13}_{-7}	1174.1	7.5×10^{-2}	34
			$8.5^{+3.5}_{-2.8} \times 10^{-4}$	264^{+100}_{-57}			
	1150.8	$2_2^+ \to 0_1^+$		$1.8^{+0.7}_{-0.4}$			0.35
1206.4	600.7[a]	$4_1^+ \to 2_1^+$		69^{+19}_{-11}	1224.2		63
1482.1	331.0	$2_3^+ \to 2_2^+$	$2.4^{+1.8}_{-0.9} \times 10^{-2}$	$9.5^{+8.5}_{-3.5}$	1549.6	4.5×10^{-2}	25
			$1.2^{+0.9}_{-0.5} \times 10^{-3}$	166^{+119}_{-61}			
	524.4	$2_3^+ \to 0_2^+$		60^{+35}_{-17}			32
	876.4	$2_3^+ \to 2_1^+$	$2.8^{+1.4}_{-0.6} \times 10^{-2}$	$3.4^{+1.9}_{-0.9}$		8.1×10^{-4}	0.4
			$1.3^{+0.6}_{-0.5} \times 10^{-4}$	30^{+16}_{-7}			
	1482.0	$2_3^+ \to 0_1^+$		$0.20^{+0.11}_{-0.05}$		0.003	
1517.3	366.5[c]	$0_3^+ \to 2_2^+$		100[d]	1661.9		100
	911.6[c]	$0_3^+ \to 2_1^+$		1.3(2)[d]		1.4	
1702.7	496.8	$4_2^+ \to 4_1^+$	<0.018	<160	1762.1	0.14	23
	551.8	$4_2^+ \to 2_2^+$		<210			39
	1097.5	$4_2^+ \to 2_1^+$		<1.1			0.6
1820.8	614.4[a]	$6_1^+ \to 4_1^+$		80^{+14}_{-10}	1851.4		88
1891.9	685.2	$3_1^+ \to 4_1^+$	$<1 \times 10^{-2}$	<4.5	1732.6	4.2×10^{-2}	12
	741.2	$3_1^+ \to 2_2^+$	$<1.8 \times 10^{-2}$	<0.7		7.9×10^{-2}	42
	1286.3	$3_1^+ \to 2_1^+$	$<1.6 \times 10^{-3}$	<0.036		7.0×10^{-4}	0.4
1976.1	273.1	$4_3^+ \to 4_2^+$	$5.3^{+2.7}_{-1.5} \times 10^{-2}$[f]		2097.7	8.1×10^{-2}	13.1
	770.0	$4_3^+ \to 4_1^+$	$1.7^{+0.9}_{-0.4} \times 10^{-3}$	27^{+11}_{-6}		4×10^{-3}	0.65
	1370.4	$4_3^+ \to 2_1^+$		$2.4^{+1.0}_{-0.6}$			0.005
2150.2	329.3	$6_2^+ \to 6_1^+$	$0.30^{+0.18}_{-0.07}$	<80	2366.4	0.18	13.8
	447.4	$6_2^+ \to 4_2^+$		82^{+58}_{-26}			64.8
	943.7	$6_2^+ \to 4_1^+$		13^{+8}_{-3}			0.8
2367.8	391.8	$5_1^+ \to 4_3^+$	$1.2^{+0.8}_{-0.4} \times 10^{-2}$		2311.2	0.13	23
	475.8	$5_1^+ \to 3_1^+$		134^{+77}_{-35}			44
	665.1	$5_1^+ \to 4_2^+$	$1.6^{+4.4}_{-0.7} \times 10^{-3}$	10^{+8}_{-5}		7.4×10^{-2}	14
	1161.2	$5_1^+ \to 4_1^+$	$1.2^{+0.7}_{-0.3} \times 10^{-4}$	$3.6^{+1.9}_{-0.9}$		2.0×10^{-3}	0.4
2573.9	753.1	$8_1^+ \to 6_1^+$		76^{+33}_{-17}	2500.1		105

TABLE III. (*Continued*)

Exp.					IBA-1		
E_{level} (keV)	Transition (keV)	$J_i^\pi \to J_f^\pi$	$B(M1)$ (W.u.)	$B(E2)$ (W.u.)	E_{level} (keV)	$B(M1)$ (W.u.)	$B(E2)$ (W.u.)
2517.4	367.1[e]	$6_3^+ \to 6_2^+$		100[d]	2670.0		
	696.3[e]	$6_3^+ \to 6_1^+$		13.3(12)[d]			
	814.6[e]	$6_3^+ \to 4_2^+$		2.9(3)[d]			
	1311.2[e]	$6_3^+ \to 4_1^+$		0.39(4)[d]			
2999.4	425.7[e]	$8_2^+ \to 8_1^+$		56(10)[d]	2997.3		10
	849.4[e]	$8_2^+ \to 6_2^+$		100[d]			100
	1178.8[e]	$8_2^+ \to 6_1^+$		3.4(2)[d]			1.1
3360.0	786.0[a]	$10_1^+ \to 8_1^+$		91^{+22}_{-20}	3178.5		112

[a]From Ref. [14].
[b]From the lifetime $\tau = 79 \pm 65$ ps reported in Ref. [10].
[c]Branching ratios from Ref. [10].
[d]Lifetime unknown, relative $B(E2)$ values are given, assuming pure $E2$ transitions.
[e]Branching ratios from Ref. [6].
[f]B value corresponding to pure transition.

the expectation is that one is able to distinguish the states with a predominantly normal configuration, which should be better described by the predictions of the model, in contrast to other states (such as, e.g., the intruder ones) which do not belong to the space of this model. The Hamiltonian used, written in the usual multipole-expanded form, was

$$H_{\text{IBA}} = \varepsilon \hat{n}_d + a_2(\hat{Q}\hat{Q})^{(0)} + a_3[(d^\dagger \tilde{d})^{(3)}(d^\dagger \tilde{d})^{(3)}]^{(0)} + a_4[(d^\dagger \tilde{d})^{(4)}(d^\dagger \tilde{d})^{(4)}]^{(0)},$$

with $\hat{Q} = (s^\dagger \tilde{d} + d^\dagger s) + \chi(d^\dagger \tilde{d})^{(2)}$, and was numerically diagonalized with the code PHINT [34] for $N_B = 9$ bosons. The parameters of this Hamiltonian were determined such as to get a reasonable description of both the level energies and their electromagnetic decays. The parameter values were the following: $\varepsilon = 0.91$ MeV, $a_2 = -0.016$ MeV, $\chi = -1.328$, $a_3 = 0.08$ MeV, and $a_4 = -0.21$ MeV. The electromagnetic decay rates were calculated with the code FBEM [34]. The quadrupole transition operator was taken the same as $\hat{Q}$, and the boson effective charge e_B, multiplying this operator, was chosen 0.1 e b. To describe the experimental electromagnetic decay branching ratios, the $M1$ transition operator was chosen as $T(M1) = g_b \hat{L} + B_1(\hat{Q}L)^{(1)}$ [35], and the parameter values (in μ_N units) were $g_b = 0.02$ and $B_1 = 0.15$.

Table III shows an extended comparison between IBA predictions and experimental data, mainly based on the $B(E2)$ strengths. When no information existed on the lifetime of the excited state, relative $B(E2)$ values are given, with the

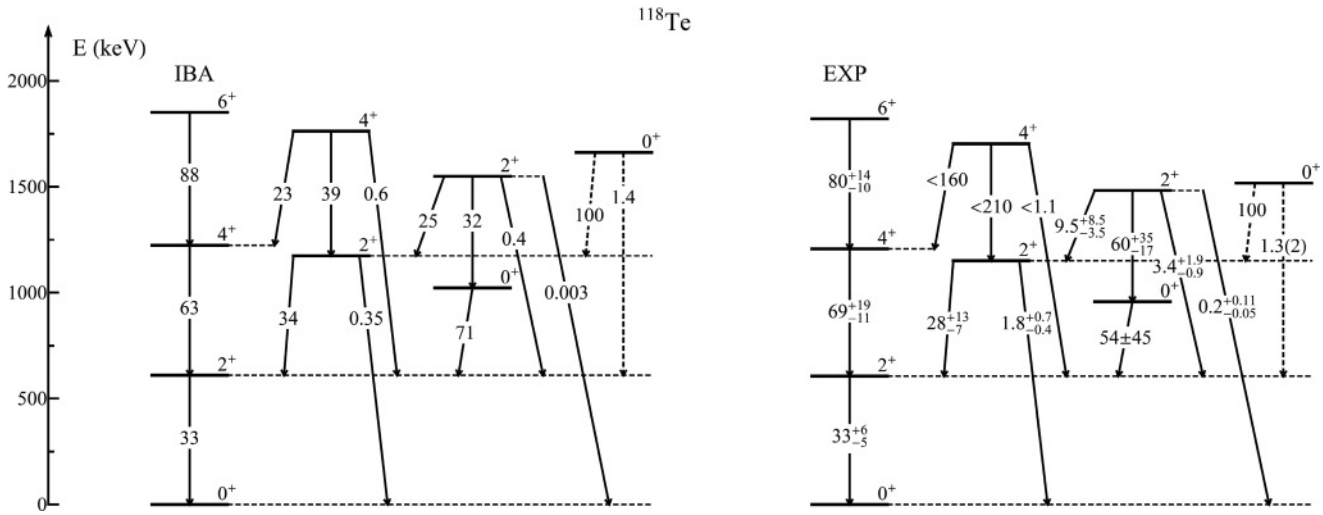

FIG. 7. Comparison between the IBA-1 model predictions (left) and experimental energies and $B(E2)$ values (right) for ^{118}Te. The transitions are labeled by the $B(E2)$ value. For the 0_3^+ level, where the absolute $B(E2)$ values are not known, the transitions are drawn with dashed arrows labeled by the relative $B(E2)$ values.

strongest value normalized to 100 (and assuming that the considered transitions are pure $E2$ transitions if their mixing ratios are not known). Figure 7 shows this comparison for the levels presumed to belong to multiphonon multiplets up to the three-phonon one.

The decay pattern of the 3_1^+ and 5_1^+ states at 1392 and 2368 keV, respectively, are not well described by the IBA-1 calculations. In fact, the experimental transition strengths confirm their assignment as two-quasiparticle states [6].

V. CONCLUSIONS

Excited states of ^{118}Te were investigated in this work with the ^{115}Te$(\alpha,n\gamma)$ reaction at 15.0 MeV incident energy, performed on a thick target. Lifetimes (or their lower limits) for most of the excited states of ^{118}Te below 2.6 MeV excitation and spin up to 8 $\hbar$ were determined by DSAM analysis of Doppler broadened γ-ray transitions. Also, the analysis of the γ-ray angular distributions measured in the same reaction provided multipolarity values $\delta(E2/M1)$ for many mixed transitions. As a result, many absolute electromagnetic transition probabilities could be determined for the low- and medium-spin, low-energy levels of this nucleus. This allowed us to investigate the character of these excited states, in connection with the possible occurrence of intruder states (due to two-proton excitations across the $Z = 50$ shell gap) in the low-energy region, and their possible mixing with the normal (vibrational) states.

A comparison of the experimental data with the IBA-1 model showed that excited states in ^{118}Te and their decay properties can be reasonably described by IBA calculations.

ACKNOWLEDGMENTS

This work was partly supported by the Romanian Ministry for Education and Research under the research projects 24-EU ISOLDE/2009, 71-042/2007, 71-051/2007, PN 09370105/2010, IDEI-181/2007, and IDEI-48/2007.

[1] P. Chowdhury, W. F. Piel Jr., and D. B. Fossan, Phys. Rev. C **25**, 813 (1982).
[2] K. Heyde, N. J. Stone, P. M. Walker, and W. B. Walters, Phys. Rep. **102**, 291 (1983).
[3] J. L. Wood, K. Heyde, W. Nazarewicz, M. Huyse, and P. van Duppen, Phys. Rep. **215**, 101 (1992).
[4] J. Rikovska, N. J. Stone, P. M. Walker, and W. B. Walters, Nucl. Phys. A **505**, 145 (1989).
[5] J. R. Vanhoy *et al.*, Phys. Rev. C **68**, 034315 (2003).
[6] S. Juutinen *et al.*, Phys. Rev. C **61**, 014312 (1999).
[7] J. R. Vanhoy *et al.*, Phys. Rev. C **69**, 064323 (2004).
[8] S. F. Hicks *et al.*, Phys. Rev. C **71**, 034307 (2005).
[9] C. Mihai *et al.*, Phys. Rev. C **81**, 034314 (2010).
[10] ENSDF, Evaluated Nuclear Structure Data File [www.nndc.bnl.gov/ensdf].
[11] P. M. Walker, C. J. Ashworth, I. S. Grant, V. R. Green, J. Rikovska, T. L. Shaw, and N. J. Stone, J. Phys. G **13**, L195 (1987).
[12] E. H. Spejewski, P. K. Hopke, and F. W. Loeser Jr., Phys. Rev. **185**, 1270 (1969).
[13] J. J. Van Ruyven, W. H. A. Hesselink, J. Akkermans, P. Van Nes, and H. Verheul, Nucl. Phys. A **380**, 125 (1982).
[14] A. A. Pasternak *et al.*, Eur. Phys. J. A **13**, 435 (2002).
[15] J. Srebrny *et al.*, Nucl. Phys. A **683**, 21 (2001).
[16] R. M. Lieder *et al.*, Eur. Phys. J. A **21**, 37 (2004).
[17] E. Grodner *et al.*, Eur. Phys. J. A **27**, 325 (2006).
[18] E. O. Lieder *et al.*, Eur. Phys. J. A **35**, 135 (2008).
[19] I. Sankowska *et al.*, Eur. Phys. J. A **37**, 169 (2008).
[20] A. A. Pasternak *et al.*, Eur. Phys. J. A **37**, 269 (2008).
[21] A. A. Pasternak, Phys. At. Nucl. **71**, 1175 (2008).
[22] E. O. Lieder *et al.*, Nucl. Instrum. Methods Phys. Res. A **607**, 591 (2009).
[23] E. Grodner *et al.*, Phys. Rev. Lett. **97**, 172501 (2006).
[24] J. Kopecky, in *Handbook for Calculations of Nuclear Reaction Data. Reference Input Parameter Library*, Chap. 6, IAEA-TECDOC-1034, August 1998 (IAEA, Vienna, 1998).
[25] S. S. Dietrich and B. L. Berman, At. Data Nucl. Data Tables **38**, 199 (1988).
[26] Yu. N. Lobach *et al.*, Acta Phys. Pol. B **30**, 1273 (1999).
[27] A. A. Pasternak *et al.*, Eur. Phys. J. A **9**, 293 (2000).
[28] J. Kopecky and M. Uhl, Report ENEA/NSC/Doc(95)1 (unpublished), p. 119.
[29] A. D. Efimov and Yu. N. Lobach, Phys. At. Nucl. **61**, 341 (1998).
[30] C. Mihai *et al.* (unpublished).
[31] T. Yamazaki, Nucl. Data Sheets A **3**, 1 (1967).
[32] T. Tamura, Nucl. Data Sheets **108**, 455 (2007).
[33] F. Iachello and A. Arima, *The Interacting Boson Model* (Cambridge University, Cambridge, England, 1987).
[34] O. Scholten, Computer codes PHINT and PBEM, KVI report Nr. 63 (unpublished).
[35] M. Ivaşcu, N. Mărginean, D. Bucurescu, I. Căta-Danil, C. A. Ur, and Yu. N. Lobach, Phys. Rev. C **60**, 024302 (1999).